Current Research in Green and Sustainable Chemistry 4 (2021) 100133

Contents lists available at ScienceDirect

Current Research in Green and Sustainable Chemistry

journal homepage: www.elsevier.com/journals/current-research-in-green-and-sustainable-chemistry/2666-0865

Nano-rod like morphology of Ni@Fe_3O_4-NDCs on interaction of NDC-supported Fe_3O_4 with nickel NPs: An efficient catalyst for ligand free Chan-Lam coupling reaction in aqueous medium

Chandan Sharma, Nitika Sharma, Shally Sharma, Surbhi Sharma, Satya Paul *

Department of Chemistry, University of Jammu, Jammu, Jammu and Kashmir, 180006, India

ARTICLE INFO

Keywords:
Nitrogen doped carbons
Magnetic nanoparticles
Nano-rods like morphology
Chan-Lam coupling
Recyclability

ABSTRACT

Nitrogen doped carbons were synthesized and fabricated with magnetite nanoparticles leading to a new magnetic and nitrogen functionalities rich carbon material. This material has dual characteristics as the magnetization of carbons makes it easily separable and the nitrogen moieties act as a binder for both magnetite and metal nanoparticles. This excludes the need for extra binding sites. Nickel and/or iron supported five different catalysts were synthesized and their catalytic activity was tested for Chan-Lam coupling and satisfactory results were obtained with two catalysts- Ni@Fe–Fe_3O_4–NDCs and Ni@Fe_3O_4–NDCs, wherein the monometallic counterpart having an upper edge. The characterization of these catalysts provides sufficient evidence for the unexpected enhanced catalytic activity of the monometallic Ni catalyst as compared to its bimetallic counterpart. The most eye-catching thing observed was the difference in morphology of the two synthesized catalysts, which clearly indicated some major changes in the interaction of the metal nanoparticles with the support material in the two catalysts since same method was adopted for the preparation of both. Additional lattice fringes of $NiFe_2O_4$ in the HRTEM images along with their corresponding peaks in the XRD spectrum, and the presence of pure Ni^{2+} species in the XPS spectrum of the monometallic catalyst provides a clear vision of the reason behind the enhanced catalytic activity of the monometallic catalyst. The formation of nano-rod like supported $NiFe_2O_4$ particles with increased surface area, mean pore volume and large number of active sites increases the activity of monometallic-Ni for Chan-Lam cross-coupling.

1. Introduction

The significant progression in nanotechnology in the past few decades has directed to remarkable applications of magnetic nanoparticles (MNPs) in diverse scientific fields, including environmental protection [1], catalysis [2,3], energy storage [4,5] and biomedicine [6,7]. MNPs as catalyst support material has been drawing significant attention as they are promptly dispersed in reaction medium with intrinsically large surface area, leading to the proficient approachability of substrates to the surface [8–11]. One of the most popular used magnetic materials, Fe_3O_4 is inexpensive, biocompatible, non-toxic and can be prepared easily [12–14]. In this regard, Fe_3O_4–supported catalytic systems have drawn significant interest owing to their remarkable properties such as a high surface area to volume ratio, ease of availability, chemical inertness and good thermal stability [15–17]. Also, Fe_3O_4-supported catalysts can be removed from the reaction medium by an external magnet, which eliminates the necessity of time-consuming and laborious filtration and centrifugation procedures [18–20]. MNPs exhibit a strong tendency to agglomerate due to self-interaction, thus, different protecting agents have been sightseen for stabilizing them. Silica [16,19,20], surfactant/-polymer [11,12], carbon-coating [18], or embedding them in a matrix/support [13] are several vibrant approaches carried out to fetch stability to these nano-structured particles. However, their coating with NDCs (carbon possessing nitrogen moieties) not only minimizes the interactions and prevents agglomeration, but also opens a way to immobilize a wide variety of metal nanoparticles as well as functionalization with organic moieties of different properties. Fe_3O_4 supported NDCs represent an excellent example of synergism of the properties of inorganic material (e.g. thermal stability, rigidity, etc) and the organic material (e.g. flexibility, processability and ductility) and thus, emerged as important tools for attaining new 'green' chemical technology.

In earlier few decades, a variety of approaches have been explored for

* Corresponding author.
E-mail address: paul7@rediffmail.com (S. Paul).

https://doi.org/10.1016/j.crgsc.2021.100133
Received 15 May 2021; Received in revised form 16 June 2021; Accepted 25 June 2021
Available online 30 June 2021

C–N coupling reaction [21] employing diverse transition metals such as Pd [22–25], Ni [26,27], Au [28,29], Cu [30,31], etc. Nowadays, interest has been focussed on 3d–transition metal NPs due to their easy availability, low cost and lesser reactivity but more selectivity in the field of catalysis. The first C–N coupling reaction was published by Fritz Ullmann [32–34] and Irma Goldberg [35] using copper catalyst but these reactions have certain limitations viz. long reaction time, high reaction temperature, limited functional group tolerance and usage of strong bases and stoichiometric quantities of copper salts. These shortcomings were knocked out by Louie and Hartwig [36], Guram et al. [37] and Surry and Buchwald [38] by utilizing palladium-based catalysts comprising palladium salts and chelating ligands. Palladium catalysts work under comprising conditions and show much tolerance to functional groups and provide high yield but suffer from toxicity and high cost. Utilization of other metals such as iron [39,40], cobalt [41–43] and nickel [26,27] has also attained interest as substitute metal catalysts to carry out C–N coupling reactions. The aspects like environment-friendly nature, ease of availability and cost-effectiveness forge them as promising catalysts for such organic transformations.

Recently, nickel-based catalysts were efficaciously employed in the C–N coupling reactions, which exhibit comparable activity to copper catalysts. Firstly, Raghuvanshi and co-workers [26] published the C–N coupling reaction of arylboronic acids with various *N*-nucleophiles using $NiCl_2{\cdot}6H_2O$, bipyridyl as ligand and DBU as base. Singh et al. [44] and Shi et al. [45] have also reported the C–N coupling using Ni(II) complexes. Lavoie and Stradiotto [27] reported the cross-coupling of NH substrates and aryl halides for the synthesis of various anilines using biphosphine ligated nickel complex and base. Keesara [46] has developed an efficient protocol for the Chan–Lam cross-coupling reactions of arylboronic acids with aryl or alkyl amines by employing simple *N*-(pyridin-2-yl)benzamide ligand with $Ni(OAc)_2.4H_2O$ in the presence of TMG as base. In all these reported methods, 15–20 mol% Ni has been used homogeneously for the synthesis of biarylamines. Consequently, it is necessary to generate simple, heterogeneous and more efficient nickel-based catalytic systems for C–N cross-coupling reactions. Nejad et al. [47] synthesized supported magnetic nickel-based heterogeneous catalyst and performed Chan-Lam reaction with amines and arylboronic acid in the presence of trisodium phosphate in water. There are very few reports of green and environmentally sustainable methodology of Chan-Lam coupling reaction using heterogeneous nickel catalyst, so there is a need of the hour to synthesize and explore the activity of nickel-based catalysts which are more active and selective.

In this report, we have synthesized eco-friendly and economical nickel and iron-based mono and bimetallic catalysts and compared their activity for Chan-Lam cross-coupling reaction and tried to explain the difference in catalytic behaviour of the respective catalysts on the basis of various characterization results. First of all, Nitrogen Doped Carbons (NDCs) were synthesized as reported in our previous work [48], and then magnetic modification was done by in situ formation of magnetite NPs on NDCs, which were then ultrasonicated for uniform distribution and proper binding. Finally, nickel and iron metal NPs were immobilized onto the magnetic NDCs in all possible combinations to get two mono-metallic, two bi-metallic and one alloy catalyst, whose catalytic activity was tested for C–N bond formation under distinct reaction conditions. We found that out of the synthesized catalysts, one monometallic Ni@Fe_3O_4–NDCs and one bimetallic catalyst Ni@Fe–Fe_3O_4–NDCs showed good activity using green and environmentally sustainable methodology. Both these catalysts were then characterized using SEM, HR-TEM, TGA, EDX, ICP-AES, VSM, BET, XPS and XRD. The unexpected enhanced catalytic behaviour of Ni@Fe_3O_4–NDCs as compared to Ni@Fe–Fe_3O_4–NDCs was explained on the basis of the morphological difference observed in the SEM images, enlarged surface area in BET, additional lattice fringes and diffraction peaks of $NiFe_2O_4$ in HRTEM and XRD respectively and finally the presence of pure Ni^{2+} species in the XPS spectrum of the monometallic catalyst, inspite of the use of reducing agent during the synthesis procedure.

2. Experimental

2.1. Materials and physical measurements

All the chemical materials utilized were bought from Aldrich Chemical Company and used further without purification. SEM images were recorded using FEG SEM JSM–7600F Scanning Electron Microscope and HR-TEM images were recorded using FEG, Tecnai G2, F30 Transmission Electron Microscope. To analyze the thermal resistance of the prepared catalysts, TGA was recorded on PerkinElmer, Diamond TG/DTA with a heating rate of 10 °C min^{-1}. EDX analysis was accomplished using OXFORD X–MAX Model JSM–7600F and the quantity of metal loaded was estimated by ICP-AES study using ARCOS, Simultaneous ICP spectrometer. For ICP-AES analysis, approx. 0.05 g of sample was taken in a microwave digestion vessel and conc. HNO_3 (4 mL), conc. HCl (2 mL) and conc. HF (2 mL) were added to it. After that the solution was diluted to 30 mL with distilled water and heated at two different temperatures. First the resulting solution was heated at 130 °C (ramp: 10 mm s) and held for 20 mm s. In the next step, the solution was heated at 190 °C (ramp: 15 mm s) and held for 20 mm s. The degree of magnetism (magnetic moment) of the prepared catalysts was estimated with a vibrating sample magnetometer (VSM) bearing Model: 7410 series, Lakeshore at room temperature from −15,000 to +15,000 Oe. BET (Brunauer–Emmett–-Teller) specific surface area was determined from N_2 adsorption-desorption isotherms at 77 K using Belsorb Mini-X analyzer. Prior to N_2 adsorption-desorption, the samples were degassed at 200 °C for 3 h under argon gas flow. XPS spectra of the catalysts were recorded on KRATOS ESCA model AXIS 165 (Resolution). XRD was recorded in 2 theta span of 10–80° on a Bruker AXSD8 Advance X-ray diffractometer deploying Cu Kα radiations. ^1H NMR (400 MHz) and ^{13}C NMR (100 MHz) spectra of the products were recorded in deuterated chloroform on Bruker Avance III spectrometer using TMS as an internal standard.

2.2. Synthesis of nitrogen doped carbons (NDCs)

Initially, we have prepared nitrogen doped carbons by heating starch:silica (1:1.2) at 553 K for 8 h in an inert atmosphere to develop an organic-inorganic hybrid composite [48]. Pyrolysis at this temperature transforms starch into activated carbon besides its interlinking with silica, which enhances its thermal stability along with the surface area. Then to raise the electron density and metal stabilizing potential, the organic-inorganic composite was doped by pyrolyzing the mixture of organic-inorganic composite and 5-phenyl-1,2,3,4-tetrazole [49] at 573 K for 6 h. The obtained nitrogen doped carbons were washed intensively with water, ethyl acetate and ethanol, and finally dried in an oven at 373 K to get the black powder.

2.3. Synthesis of Fe_3O_4 grafted nitrogen doped carbons (Fe_3O_4-NDCs)

Ultrasonication of the NDCs (1 g) obtained in the first step was carried out in 50 mL of deionized water for 30 min. Afterward, the in situ chemical co-precipitation of Fe^{3+} and Fe^{2+} -ions with a molar ratio of 2:1 was done [50,51]. The aqueous solution of $FeSO_4{\cdot}7H_2O$ (0.3 g, 1.079 mmol) and $Fe_2(SO_4)_3$ (0.4314 g, 1.079 mmol) was added to the NDCs solution and the resultant suspension was stirred at 85 °C under nitrogen atmosphere. Subsequently, NH_4OH solution (2–3 mL) was added gradually into the reaction mixture, which results in the instant generation of black precipitates of Fe_3O_4 MNPs and the stirring was continued for another 2 h. The Fe_3O_4–NDCs so formed was separated by magnetic decantation and washed several times with deionized water (3 × 15 mL) and ethanol (3 × 15 mL) followed by drying in an oven at 373 K to get the light brick-red color powder.

2.4. Synthesis of nickel/iron immobilized Fe_3O_4-NDCs catalysts

Ni and Fe nanoparticles were separately immobilized onto

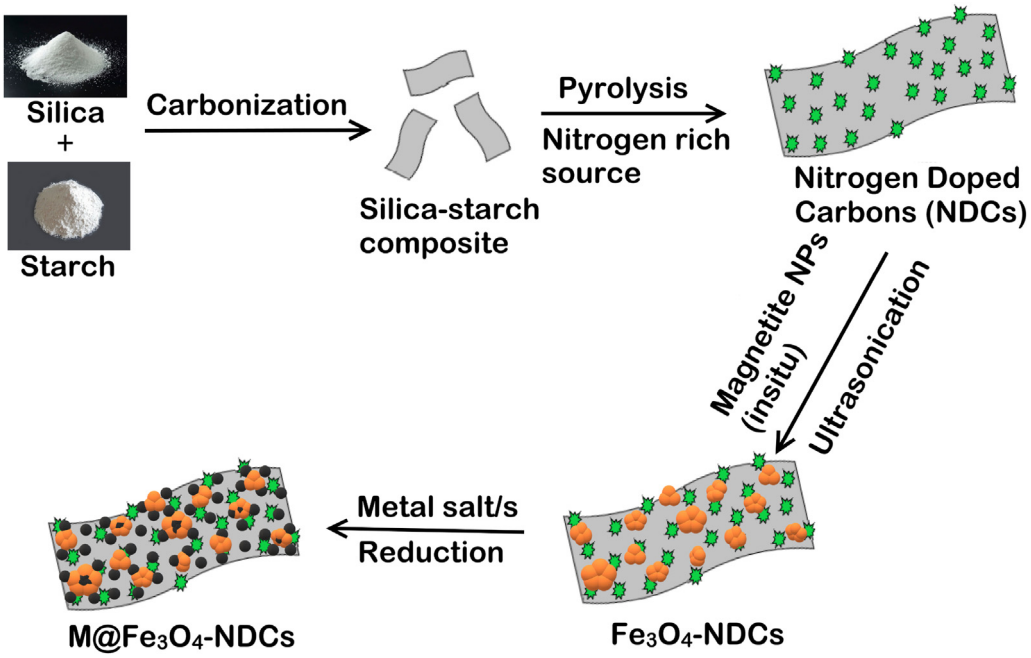

Scheme 1. General scheme for the synthesis of metal NPs immobilized on magnetically modified nitrogen doped carbons.

Fe_3O_4–NDCs support to get two different monometallic catalysts: Ni@Fe_3O_4–NDCs and Fe@Fe_3O_4–NDCs. Firstly, the support material (Fe_3O_4–NDCs, 1 g) was stirred in deionized water (20 mL) for 30 min followed by the dropwise addition of the solution of $NiCl_2{\cdot}6H_2O$ (118.8 mg, 0.5 mmol) in 5 mL deionized water and stirring was continued for 2 h. After this, a freshly prepared $NaBH_4$ solution in water (1.0 mmol, 5 mL) was added dropwise while stirring at room temperature which was continued for 8 h to get the nickel-based monometallic catalyst. The prepared catalyst Ni@Fe_3O_4–NDCs was separated by magnetic decantation and then thoroughly washed with ethyl acetate (3 × 15 mL), deionized water (3 × 15 mL) and ethanol (3 × 15 mL) to eliminate the unbound material. Similarly, Fe@Fe_3O_4–NDCs was prepared using the same procedure as mentioned above, but here $FeSO_4{\cdot}7H_2O$ (139 mg, 0.5 mmol) was used instead of nickel salt.

2.5. Synthesis of nickel and iron immobilized Fe_3O_4-NDCs catalysts

Three different types of Ni–Fe based bimetallic catalysts were synthesized based on the stepwise and simultaneous addition of corresponding metal salts. To synthesize Ni@Fe–Fe_3O_4–NDCs, the support material (Fe_3O_4–NDCs, 1 g) was stirred in deionized water (20 mL) for 30 min followed by the dropwise addition of the solution of $FeSO_4{\cdot}7H_2O$ (139 mg, 0.5 mmol) in 5 mL deionized water. After 2 h stirring at room temperature, dropwise addition of a freshly prepared $NaBH_4$ solution in water (1.0 mmol, 5 mL) was done succeeded by 2 h additional stirring at room temperature. Next step involves the dropwise addition of $NiCl_2{\cdot}6H_2O$ solution (118.8 mg, 0.5 mmol) in 5 mL deionized water followed by stirring for 2 h and subsequent reduction using a freshly prepared $NaBH_4$ solution in water (1.0 mmol, 5 mL). The reaction mixture was stirred for additional 8 h at room temperature to get Ni@Fe–Fe_3O_4–NDCs. The prepared catalyst, Ni@Fe–Fe_3O_4–NDCs was isolated by magnetic decantation and washed with ethyl acetate (3 × 15 mL), deionized water (3 × 15 mL) and ethanol (3 × 15 mL) to eliminate the unbound material. Similarly, Fe@Ni–Fe_3O_4–NDCs was synthesized following the same method as mentioned above, but in this case nickel salt was added prior to iron salt. And the synthesis of NiFe@Fe_3O_4–NDCs was also carried out adopting the similar procedure in which both the salts were added simultaneously.

2.6. Chan-Lam cross-coupling

The mixture of arylamine (1 mmol), arylboronic acid (1 mmol), K_2CO_3 (1 eq.) and Ni@Fe_3O_4–NDCs (0.1 g) in deionized water (5 mL) was stirred at 100 °C and the progression of the reaction was examined via TLC. After the end of the reaction, the mixture was left to cool down and the catalyst was recovered using an external magnet, washed with ethyl acetate (3 × 5 mL), deionized water (2 × 10 mL) and dried under vacuum, while the reaction mixture was diluted with water and the crude product was extracted with ethyl acetate (3 × 5 mL). The combined extracts were then washed with a brine solution followed by drying over anhydrous Na_2SO_4. The crude product was purified with column chromatography using silica gel (60–120 mesh) with a solution of petroleum ether and ethyl acetate as an eluent to furnish the desired *N*-arylated product.

The identification and purity of all the products was confirmed by ^1H and ^{13}C NMR spectral data and comparison with reliable samples obtained commercially or synthesized according to the literature approaches.

3. Results and discussion

3.1. Characterization

In the present work, we have synthesized eco-friendly, economical and magnetically recoverable five different catalysts, Fe@Fe_3O_4–NDCs, Fe@Ni–Fe_3O_4–NDCs, NiFe@Fe_3O_4–NDCs, Ni@Fe_3O_4–NDCs and Ni@Fe–Fe_3O_4–NDCs. The schematic representation of the preparation of these catalysts is shown in Scheme 1. Initially, we have synthesized composite carbon material from silica and starch to increase thermal stability as well as surface area, followed by its modification with a nitrogen rich source to get nitrogen doped carbons (NDCs). Fe_3O_4 nanoparticles were prepared in situ on NDCs by the co-precipitation of Fe^{2+} and Fe^{3+} salts followed by dispersion of magnetite nanoparticles using ultrasonication. Finally, metal nanoparticles were immobilized onto Fe_3O_4–NDCs composite using metal salts followed by reduction with aqueous sodium borohydride solution. First of all, the catalytic activity of the synthesized catalysts was tested for C–N bond formation between aniline and phenylboronic acid using green and environmentally

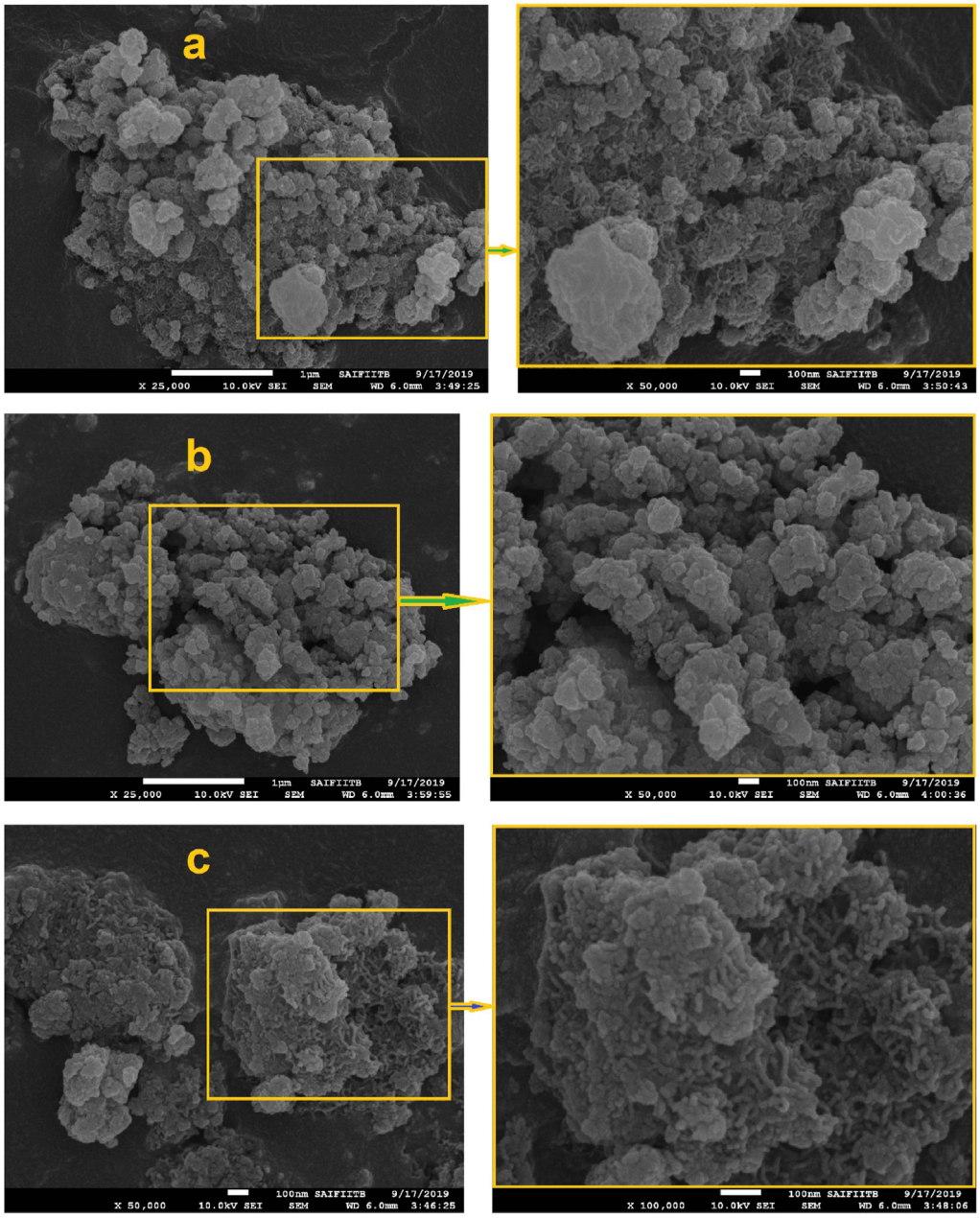

Fig. 1. SEM images of Ni@Fe_3O_4–NDCs (a,c) and Ni@Fe–Fe_3O_4–NDCs (b).

sustainable methodology and the most active catalysts, Ni@Fe_3O_4–NDCs and Ni@Fe–Fe_3O_4–NDCs were fully characterized using various techniques, such as SEM, HR-TEM, TGA, EDX, ICP-AES, VSM, BET, XPS and XRD.

Microscopic images of the catalysts were captured using a scanning electron microscope (SEM) and the morphology was precisely investigated. A clear difference is observed in the morphology of Ni@Fe_3O_4–NDCs and Ni@Fe–Fe_3O_4–NDCs. Nano-rods like structures [52] were observed in the SEM images of Ni@Fe_3O_4–NDCs (Fig. 1a,c), whereas agglomerated quasi spherical shape was observed for the bimetallic catalyst (Fig. 1b). This clearly indicated the variable interaction of metal NPs with support material in the two catalysts since the method of preparation adopted was same in both the cases.

To gain further insight into the morphology and distribution of Fe_3O_4 as well as metal nanoparticles onto NDCs, HR-TEM of Ni@Fe_3O_4–NDCs and Ni@Fe–Fe_3O_4–NDCs catalysts were recorded (Fig. 2). The brilliant black spots in Fig. 2 most likely showed the uniform distribution of metal NPs as well as ferrites onto the surface of NDCs.

Well defined lattice fringes corresponding to Ni NPs [53,54] and Fe_3O_4 [55–57] were observed in both the catalysts. Further, additional lattice fringe corresponding to (100) plane of metallic iron was found in the bimetallic catalyst [58]. To our surprise, Fig. 2g,h displayed some unexpected lattice fringes with interplanar spacing of about 0.25 nm, 0.31 nm and 0.418 nm corresponding to (311), (220) and (111) planes of $NiFe_2O_4$ (JCPDS card no. 03–0875), whereas no such results were found in bimetallic catalyst [59]. This advocates that the morphological difference in SEM was due to the formation of nickel ferrites in Ni@Fe_3O_4–NDCs. Thus, the HR-TEM images confirmed the successful immobilization of respective metal and ferrites nanoparticles on the NDCs and also provide the sufficient evidence regarding the difference in catalysts morphology.

The thermogravimetric analysis (TGA) curves of Fe_3O_4–NDCs, Ni@Fe_3O_4–NDCs and Ni@Fe–Fe_3O_4–NDCs are represented in Fig. 3. The initial weight loss occurs up to 130 °C, which can be ascribed to the

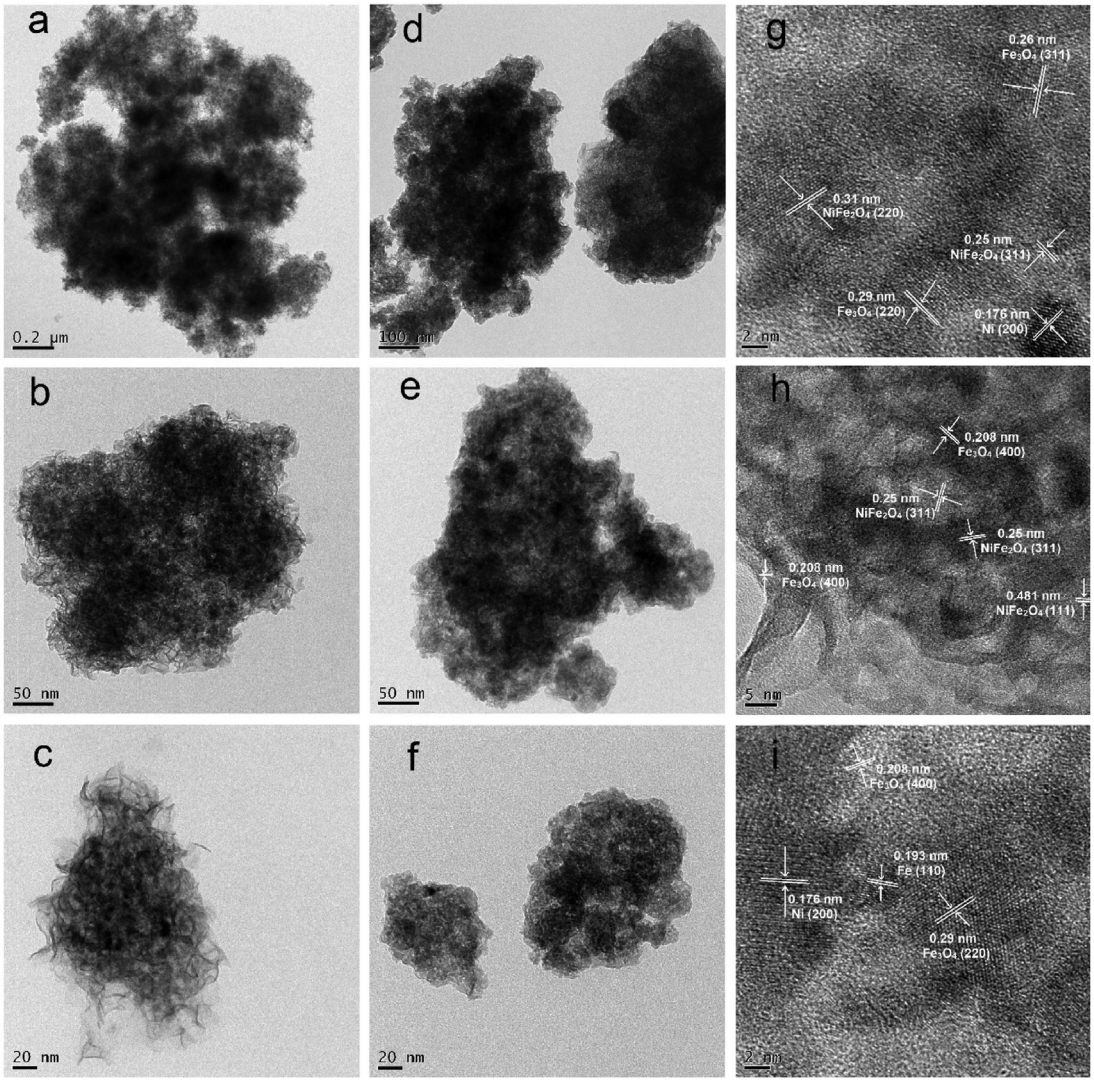

Fig. 2. HR-TEM images of Ni@Fe_3O_4–NDCs (a,b,c,g,h) and Ni@Fe–Fe_3O_4–NDCs (d,e,f,i).

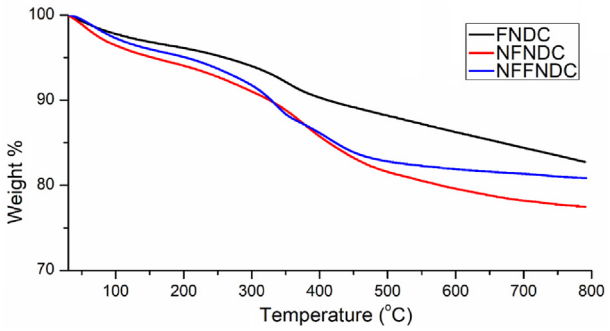

Fig. 3. TGA plot of Fe_3O_4–NDCs (FNDC), Ni@Fe_3O_4–NDCs (NFNDC) and Ni@Fe–Fe_3O_4–NDCs (NFFNDC).

elimination of entrapped solvent and water molecules on the surface of these composite materials. Afterward, there is no noticeable weight loss till 200 °C, which confers that the catalysts as well as support material are stable up to 200 °C.

Further, slight weight loss is observed up to 300 °C and then sudden weight loss of 10–12 wt% up to 450 °C takes place, which may be due to initial slow decomposition and then the complete collapse of carbonaceous material present in the composite support material. We observed swift decomposition of carbonaceous material in both the catalysts because of the catalytic nature of impregnated metal nanoparticles, which not only decrease the activation energy but also accelerate the decomposition of carbons [60,61]. Later, there is no further weight loss until 800 °C as only stable oxides are left. The residual weight of about 80–85% represented the weight of ferrites, silica and metal oxides. These results illustrate that the synthesized catalysts can be efficiently used for carrying out the organic transformations up to 200 °C without any substantial loss in catalytic activity.

The elemental composition in synthesized catalysts was confirmed by energy dispersive X-ray spectroscopy (EDX), which authorizes the presence of C, N, O, Fe, Ni and Si in both the catalysts. All the elements are present according to various materials used in their preparation (Fig. 4) and eliminate the possibility of any type of contamination in them. Also, the peak intensities confirmed the proper binding of metal nanoparticles according to their quantities used. To estimate the content of Ni and Fe immobilized onto magnetic NDC support, the catalyst was analyzed using inductively coupled plasma atomic emission spectroscopy (ICP-AES). It was found that the content of nickel was 2.17 and 2.04 wt%, whereas the amount of Fe was found to be 15.81 and 17.54 wt% in Ni@Fe_3O_4–NDCs and Ni@Fe–Fe_3O_4–NDCs respectively. In the monometallic counterpart, the presence of 15.81 wt% Fe reveals the amount of embedded Fe_3O_4 NPs on NDCs. However, in its bimetallic counterpart, this value enhances to

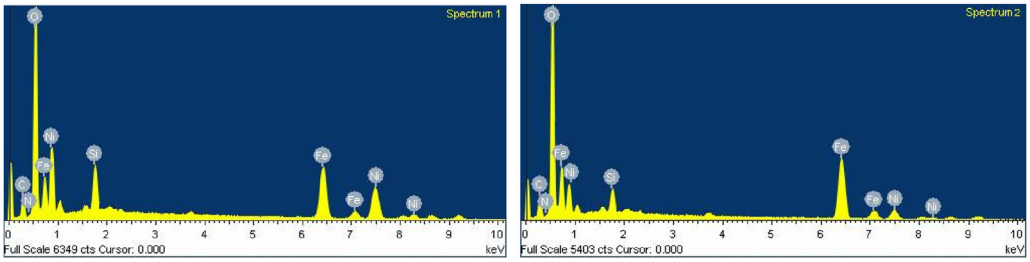

Fig. 4. EDX of Ni@Fe_3O_4–NDCs (spectrum 1) and Ni@Fe–Fe_3O_4–NDCs (spectrum 2).

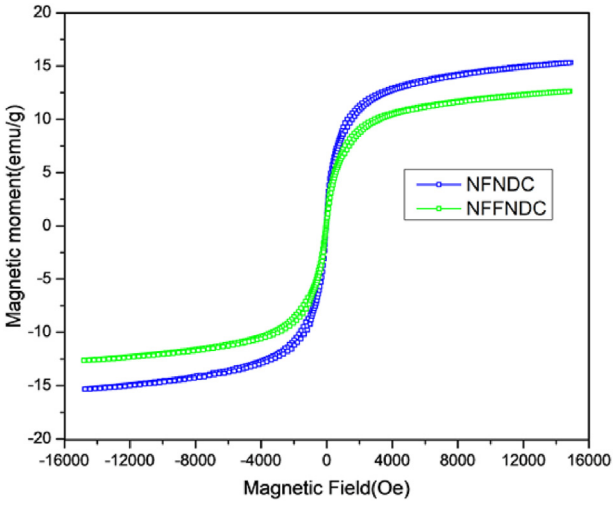

Fig. 5. VSM plot of Ni@Fe_3O_4–NDCs (NFNDC) and Ni@Fe–Fe_3O_4–NDCs (NFFNDC).

17.54 wt % with an increment of 1.73 wt% which suggests that loading of metallic Fe took place successfully.

The purpose of the introduction of MNPs is to sightsee the potential reusability of the catalysts. In this context, the magnetic properties of the synthesized catalysts were investigated with vibrating sample magnetometer (VSM) at room temperature. The magnetic hysteresis loops of Ni@Fe_3O_4–NDCs and Ni@Fe–Fe_3O_4–NDCs are represented in Fig. 5, which shows that both these catalysts unveiled characteristic features of ferromagnetism and thus are magnetic enough to be separated via magnet at room temperature [62]. The value of magnetization saturation of Ni@Fe_3O_4–NDCs and Ni@Fe–Fe_3O_4–NDCs were found to be 15.33 and 12.64 emu/g respectively. This fall in the magnetization saturation value as compared to the reported bare Fe_3O_4 nanoparticles [63] can be attributed to the uniform grafting of Fe_3O_4 nanoparticles on NDCs as well as their coating with the metal nanoparticles. Nevertheless, the magnetic saturation of these catalysts still holds a high value, which ensured the quick and complete separation of the synthesized catalysts from reaction mixture using a permanent magnet.

The textural properties of the catalysts were depicted by N_2 adsorption-desorption measurements. Fig. 6 displayed that both the catalysts have a similar type–IV isotherm with a hysteresis loop at high relative pressures, demonstrating the mesoporous nature of the catalysts. The size of the hysteresis loop of Ni@Fe_3O_4–NDCs is almost double as compared to that of Ni@Fe–Fe_3O_4–NDCs, which indicate that the former has higher porosity.

The specific surface areas, pore volumes and mean pore diameters of Ni@Fe_3O_4–NDCs and Ni@Fe–Fe_3O_4–NDCs are estimated using the Brunauer–Emmett–Teller (BET) method and are summarized in Table 1. The pore size distribution was analyzed by Barrett–Joyner–Halenda (BJH) plots (Fig. S1, **Supplementary data**) and it was found that Ni@Fe_3O_4–NDCs shows broader BJH pore size distribution than Ni@Fe–Fe_3O_4–NDCs due to its larger particle size. The combined results of BET and BJH confirmed the improved textural properties of Ni@Fe_3O_4–NDCs, as also evident from the SEM micrographs (Fig. 1), which can expedite the accessibility of surface-active sites.

XPS study was carried out to examine the surface species existing in the synthesized catalysts. Fig. S2 (**Supplementary data**) presents the

Table 1
Various structural parameters analyzed via BET analysis of Ni@Fe_3O_4–NDCs and Ni@Fe–Fe_3O_4–NDCs

S. No.	Catalyst	Surface area ($m^2\ g^{-1}$)	Pore volume ($cm^3\ g^{-1}$)	Mean pore diameter (nm)
1.	Ni@Fe_3O_4–NDCs	269.26	0.4721	7.0138
2.	Ni@Fe–Fe_3O_4–NDCs	214.08	0.2280	4.2604

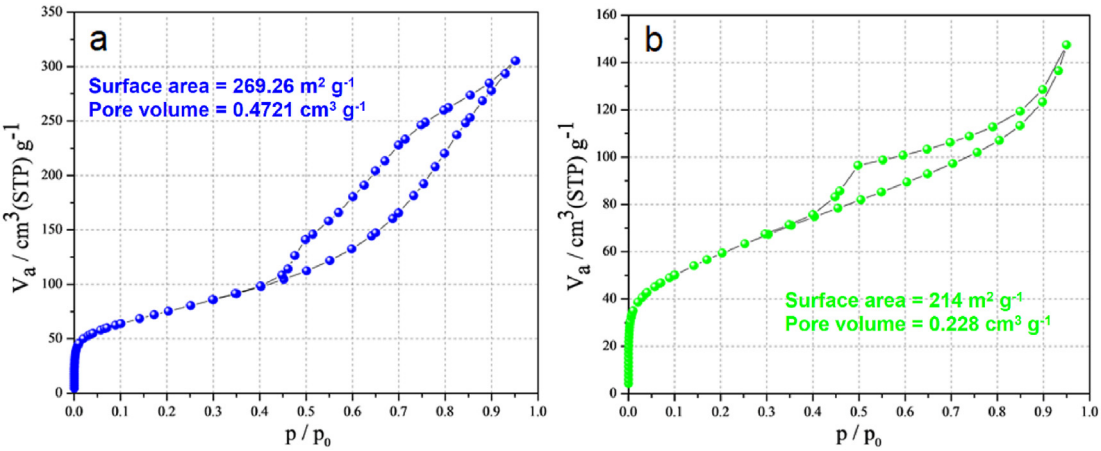

Fig. 6. Adsorption-desorption isotherm of a) Ni@Fe_3O_4–NDCs and b) Ni@Fe–Fe_3O_4–NDCs.

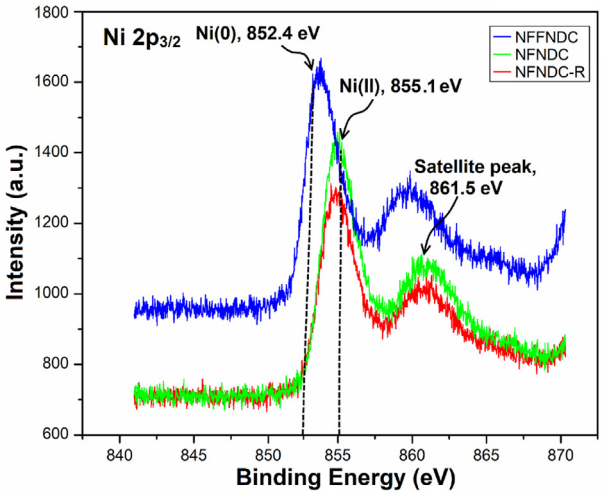

Fig. 7. Ni $2p_{3/2}$ XPS spectra of Ni@Fe_3O_4–NDCs (NFNDC, green), after six consecutive runs (NFNDC-R, red) and Ni@Fe–Fe_3O_4–NDCs (NFFNDC, blue). (For interpretation of the references to color in this figure legend, the reader is referred to the Web version of this article.)

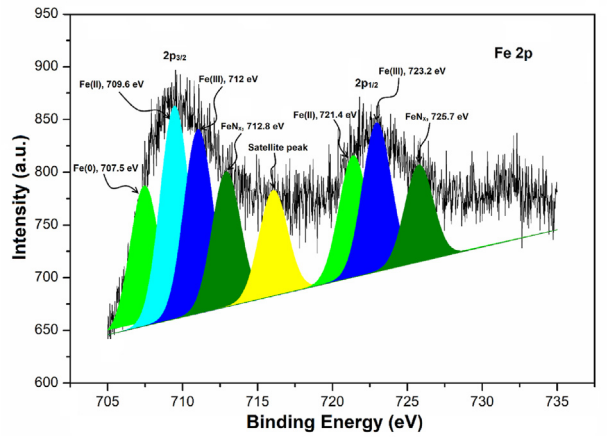

Fig. 8. Fe 2p XPS spectra of Ni@Fe–Fe_3O_4–NDCs.

full-scan comparative XPS spectra of Ni@Fe_3O_4–NDCs (fresh and reused) and Ni@Fe–Fe_3O_4–NDCs and Fig. 7 exhibits the binding energies (BEs) of Ni $2p_{3/2}$ species. The dotted vertical lines at 852.4 and 855 eV represent the BEs of Ni(0) and Ni(II) species according to literature report [59,64,65]. We see from Ni $2p_{3/2}$ BEs that Ni@Fe–Fe_3O_4–NDCs contains mainly Ni(0) species with little bit Ni(II), which could be attributed to surface oxidation. However, the XPS spectrum of Ni@Fe_3O_4–NDCs shows some interesting results which were quite different from the ideal results. Ni@Fe_3O_4–NDCs catalyst was found to contain pure Ni(II) species without any evidence of Ni(0) which was somewhat surprising since both the catalysts were prepared by using the same synthetic procedure. The additional satellite peak at around 861.5 eV confirms that nickel is present in +2 oxidation state in Ni@Fe_3O_4–NDCs [65]. The appearance of Ni(II) species in monometallic counterpart, despite of the reduction with sodium borohydride in their synthesis, authenticates the formation of nickel ferrites ($NiFe_2O_4$), which in turn is responsible for the improved morphology, enhanced surface area and improved catalytic activity.

Further, to check the stability of the monometallic catalyst, XPS of reused catalyst was recorded and results indicated that there is no change in the electronic environment around Ni^{2+}-ions even after six catalytic runs.

Fig. 8 shows BEs of Fe $2p_{3/2}$ species in Ni@Fe–Fe_3O_4–NDCs. In

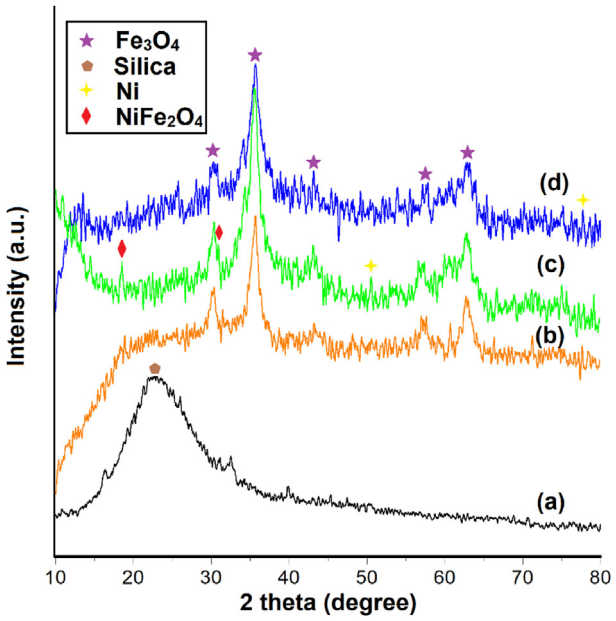

Fig. 9. Comparative XRD pattern of: (a) NDCs, (b) Fe_3O_4–NDCs, (c) Ni@Fe_3O_4–NDCs and (d) Ni@Fe–Fe_3O_4–NDCs.

contrast to Ni, Fe in catalysts was present in varied oxidation states extending from 0 to +3 and thus, it can be a challenge to find out the accurate oxidation states of Fe present in Ni@Fe–Fe_3O_4–NDCs. The elucidation of the BEs of Fe 2p in Fig. 8 was drawn after contemplation of copious literature reports [64,66]. Deconvolution of Fe 2p spectra show peaks at the binding energies of 707.5 eV, 709.6 eV, 712 eV, 712.8 eV, 716.5 eV, 721.4 eV, 723.5 eV and 725.7 eV. A small peak at 707.5 eV shows the presence of Fe(0) species, while a peak at 709.6 eV corresponds to Fe(II) species and a peak at 712 eV is assigned to $2p_{3/2}$ region of Fe(III) species in Fe_3O_4. The peak at 716.5 eV has been recognized as a satellite peak symbolizing Fe $2p_{3/2}$. The peak at 712.8 eV is ascribed to FeN_x $2p_{3/2}$, whereas the peaks at 721.4 eV, 723.2 eV and 725.7 eV are ascribed to $2p_{1/2}$ region of Fe(II), Fe(III) and FeN_x respectively.

Comparative X-ray diffraction analysis (XRD) was done to investigate the successful grafting of Fe_3O_4 on NDCs and respective metal nanoparticles on Fe_3O_4–NDCs. Fig. 9 shows the XRD patterns of nitrogen doped carbons (NDCs), magnetite grafted nitrogen doped carbons (Fe_3O_4–NDCs) and two of the synthesized catalysts, Ni@Fe_3O_4–NDCs and Ni@Fe–Fe_3O_4–NDCs. In the NDCs XRD pattern (Fig. 9a), only a broad peak was observed at $2\theta \approx 22°$ due to the amorphous silica matrix [67]. The remaining three XRD patterns exhibited almost similar diffraction patterns except for a few peaks of nickel ferrite in monometallic catalyst and metallic nickel in both the catalysts. The diffraction patterns appearing at $2\theta = 30.1°$, 35.71°, 43.19°, 57.4° and 62.9° are ascribed to the scattering due to (220), (311), (400), (511) and (440) lattice planes of cubic Fe_3O_4 (JCPDS No. 65–3107) [68]. Further, a small diffraction peak corresponding to (220) crystalline plane of cubic metallic Ni appeared at $2\theta = 76.3°$ in both the catalysts (Fig. 9c,d), however another small diffraction peak of cubic metallic Ni was observed in Ni@Fe_3O_4–NDCs (Fig. 9c) at $2\theta = 51.5°$ corresponding to (200) crystalline plane [69,70]. The appearance of a weak Ni signal symbolized that the Ni nanoparticles were well spread onto the surface of the support material. The absence of diffraction patterns of metallic Fe in Ni@Fe–Fe_3O_4–NDCs (Fig. 9d) might be due to its uniform dispersion or its overlap with Fe_3O_4 diffraction patterns and $NiFe_2O_4$ (JCPDS 10–0325) [71,72]. Two additional peaks at 18.4° and 30.4° are observed in Ni@Fe_3O_4–NDCs (Fig. 9c) which could be ascribed to (111) and (220) planes of $NiFe_2O_4$ (JCPDS 10–0325) [71,72]. However, no such peaks are observed in the XRD spectrum of Ni@Fe–Fe_3O_4–NDCs (Fig. 9d) thereby excluding any possibility of nickel ferrite species in it. Further, the other diffraction peaks of $NiFe_2O_4$ are not

Table 2
Effect of catalyst, base, solvent and temperature in C–N cross-coupling between aniline and phenylboronic acid[a]

Entry	Catalyst (g)	Base (eq.)	Solvent	Temperature (°C)	Time (h)	Yield[b] (%)
1	NiFe@Fe_3O_4–NDCs (0.1)	K_2CO_3(1)	H_2O	80	12	Trace
2	Ni@Fe–Fe_3O_4–NDCs (0.1)	K_2CO_3(1)	H_2O	80	9	44
3	Fe@Ni–Fe_3O_4–NDCs (0.1)	K_2CO_3(1)	H_2O	80	15	NR
4	Fe@Fe_3O_4–NDCs (0.1)	K_2CO_3(1)	H_2O	80	15	NR
5	Ni@Fe_3O_4–NDCs (0.1)	K_2CO_3(1)	H_2O	80	6	74
6	Ni@Fe–Fe_3O_4–NDCs (0.1)	-	H_2O	80	9	16
7	Ni@Fe_3O_4–NDCs (0.1)	-	H_2O	80	6	38
8	Ni@Fe–Fe_3O_4–NDCs (0.1)	CH_3COONa(1)	H_2O	80	9	32
9	Ni@Fe_3O_4–NDCs (0.1)	CH_3COONa(1)	H_2O	80	6	55
10	Ni@Fe–Fe_3O_4–NDCs (0.1)	Na_2CO_3(1)	H_2O	80	9	38
11	Ni@Fe_3O_4–NDCs (0.1)	Na_2CO_3(1)	H_2O	80	6	62
12	Ni@Fe–Fe_3O_4–NDCs (0.1)	K_2CO_3(1)	DMF	80	9	26
13	Ni@Fe_3O_4–NDCs (0.1)	K_2CO_3(1)	DMF	80	6	40
14	Ni@Fe–Fe_3O_4–NDCs (0.1)	K_2CO_3(1)	EtOH	80	9	42
15	Ni@Fe_3O_4–NDCs (0.1)	K_2CO_3(1)	EtOH	80	6	62
16	Ni@Fe–Fe_3O_4–NDCs (0.1)	K_2CO_3(1)	CH_3CN	80	9	34
17	Ni@Fe_3O_4–NDCs (0.1)	K_2CO_3(1)	CH_3CN	80	6	51
18	Ni@Fe_3O_4–NDCs (0.1)	K_2CO_3(1)	H_2O	RT	15	52
19	Ni@Fe_3O_4–NDCs (0.1)	K_2CO_3(1)	H_2O	60	12	68
20	**Ni@Fe_3O_4–NDCs (0.1)**	**K_2CO_3(1)**	**H_2O**	**100**	**3**	**86**
21	Ni@Fe_3O_4–NDCs (0.1)	K_2CO_3(1)	H_2O	100	6	88
22	Ni@Fe_3O_4–NDCs (0.05)	K_2CO_3(1)	H_2O	100	3	54
23	Ni@Fe_3O_4–NDCs (0.2)	K_2CO_3(1)	H_2O	100	3	89
24	Ni@Fe_3O_4–NDCs (0.1)	K_2CO_3(0.5)	H_2O	100	3	52
25	Ni@Fe_3O_4–NDCs (0.1)	K_2CO_3(2)	H_2O	100	3	87
26	Ni@Fe–Fe_3O_4–NDCs (0.1)	K_2CO_3(1)	H_2O	100	3	48
27	Fe_3O_4–NDCs (0.1)	K_2CO_3(1)	H_2O	100	6	NR
28	–	K_2CO_3(1)	H_2O	100	6	NR

[a] Reaction conditions: phenyl boronic acid (1 mmol), aniline (1 mmol), base, catalyst and solvent (5 mL).
[b] Column chromatography yield.

distinguishable in Ni@Fe_3O_4–NDCs (Fig. 9c) due to their close proximity with the diffraction peaks of Fe_3O_4.

Also, the particle size was evaluated using Scherrer equation and it came out to be 6.02 and 4.35 nm for Ni@Fe_3O_4–NDCs and Ni@Fe–Fe_3O_4–NDCs respectively. These findings are in well agreement with BJH plot results.

Thus, it was the morphological difference of two active catalysts observed in SEM that provides us the basic idea behind the enhanced catalytic activity of Ni@Fe_3O_4–NDCs. This inculcates the curiosity to explore the reason behind the difference in morphology despite following the same procedure in the preparation of all the catalysts. HRTEM provides the right path in this direction by signalling the formation of nickel ferrites in Ni@Fe_3O_4–NDCs as evident from their respective lattice fringes. This was further supported by the XPS spectra of the respective catalysts. The bimetallic catalyst was found to contain Ni(0) as a major species with small amounts of Ni(II). The lower percentage of Ni(II) in bimetallic catalyst could be attributed to surface oxidation. However, the XPS spectrum of monometallic Ni catalyst showed unexpected results as it contained pure Ni(II) species despite adopting the same method of preparation in both the cases. This in a way confirmed the formation of supported nickel ferrites in the monometallic catalyst. Finally, XRD also shows additional diffraction peaks corresponding to $NiFe_2O_4$ in Ni@Fe_3O_4–NDCs, whereas no such peaks were found in bimetallic counterpart. Hence, all the studies discussed above authenticated the interaction of Ni NPs with the supported Fe_3O_4 NPs thereby forming supported nickel ferrite, which resulted in improved morphology and enhanced catalytic activity of Ni@Fe_3O_4–NDCs.

3.2. Catalytic testing for C–N bond formation

Substituted diarylamines have gained appreciable attention due to their diverse applicability in natural products and medicinal chemistry. The catalytic activity of the synthesized catalysts has been evaluated for the C–N coupling reaction using phenyl boronic acid and aniline as test substrates. We have tested all the synthesized catalysts for the test reaction and summarized the results in Table 2. As shown in Table 2, out of five prepared mono- as well as bimetallic catalysts, Ni@Fe_3O_4–NDCs and Ni@Fe–Fe_3O_4–NDCs showed good catalytic activity. Both these catalysts were scanned for the test reaction with different bases (Na_2CO_3, CH_3COONa and K_2CO_3). In the absence of base, both the catalysts gave very less yield in aqueous conditions (Table 2, entries 6 and 7) which indicated that base played an important part in C–N coupling reaction as it triggers the phenyl boronic acid during the reaction. We have also studied the effect of several bases (Table 2, entries 2, 5, 8–11) and found that out of various inorganic bases examined (Na_2CO_3, CH_3COONa and K_2CO_3), K_2CO_3 gave the most reliable results concerning reaction time and yield (Table 2, entries 2 and 5). Before optimizing the amount of base, we optimized solvent, temperature and amount of catalyst. The activity of Ni@Fe_3O_4–NDCs and Ni@Fe–Fe_3O_4–NDCs was tested in case of the test reaction using various solvents (H_2O, EtOH, CH_3CN and DMF) in the presence of K_2CO_3 at 80 °C (Table 2, entries 2, 5, 12–17) and water was found to be the best solvent due to the good stability of phenyl boronic acid. Out of these two catalysts, Ni@Fe_3O_4–NDCs showed better activity in all the conditions as compared to its bimetallic counterpart. Further, temperature of the reaction was optimized using the best catalyst (Ni@Fe_3O_4–NDCs) in the selected reaction conditions (Table 2, entries 18–20) and it has been found that the reaction gave the best results at 100 °C. Lastly, the catalyst and base amounts were screened as well (Table 2, entries 22–25) and observed that 0.1 g of catalyst and 1 eq. of K_2CO_3 were the appropriate amounts to catalyze the C–N coupling reaction efficiently. To authenticate the role of nickel nanoparticles, we have performed the test reaction in the presence of Fe_3O_4-NDCs (Table 2, entries 27) as well as in the absence of any catalyst (Table 2, entries 28) using the optimized reaction conditions and no reaction was observed in both the cases, which confirms that nickel nanoparticles are the active species for catalyzing C–N couplings. Thus, after carrying out various experiments, we concluded that out of five synthesized catalysts, Ni@Fe_3O_4–NDCs gave the best results using water as reaction medium, K_2CO_3 (1 eq.) as the base and catalyst (0.1 g) at 100 °C (Table 2, entry 20).

The scope of magnetically recoverable catalyst, Ni@Fe_3O_4–NDCs was further extended using green and environmentally sustainable

Table 3
Ni@Fe_3O_4–NDCs catalyzed C–N cross-coupling reaction between amines and arylboronic acids in water[a]

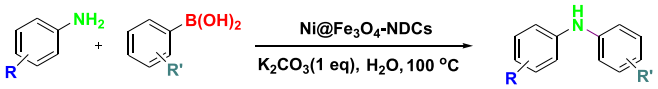

Entry	Amine Compounds	Boronic Acids	Product	Time (h)	Yield[b] (%)
1	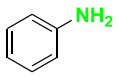	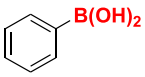	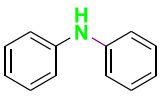	3	86
2	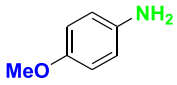	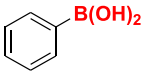	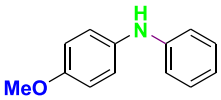	3	89
3	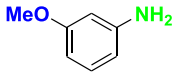	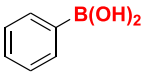	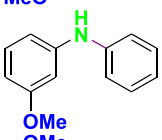	6	80
4	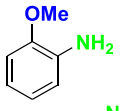	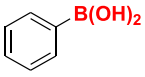	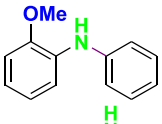	9	60
5	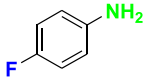	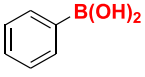	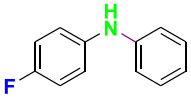	4	86
6	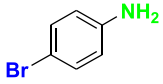	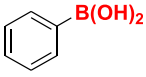	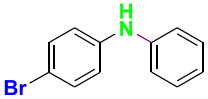	4	78
7	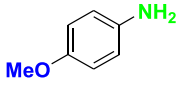	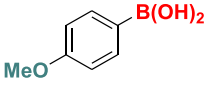	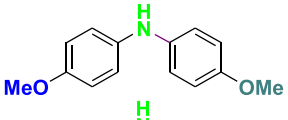	4	79
8	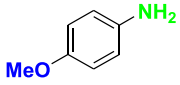	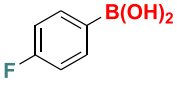	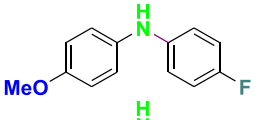	3	85
9	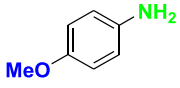	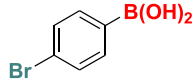	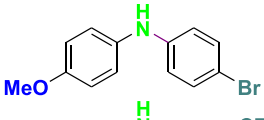	4	75
10	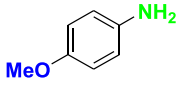	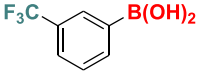	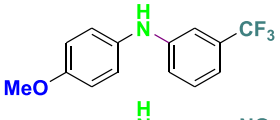	5	74
11	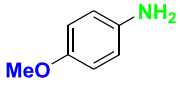	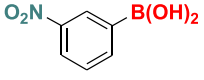	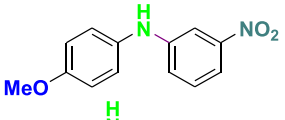	3	76
12	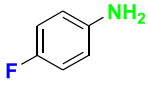	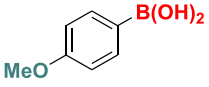	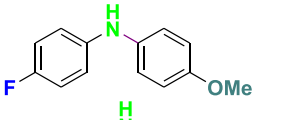	4	75
13	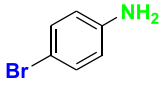	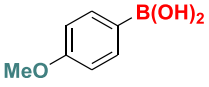	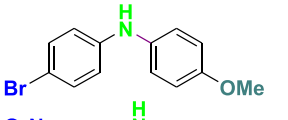	5	75
14				6	72
15				4	80
16				4	84

(*continued on next page*)

Table 3 (*continued*)

Entry	Amine Compounds	Boronic Acids	Product	Time (h)	Yield[b] (%)
17	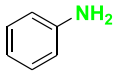	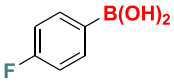	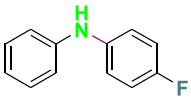	4	83
18		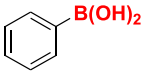	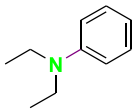	9	Trace
19	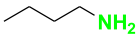	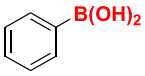	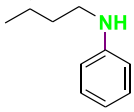	9	Trace
20		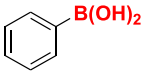	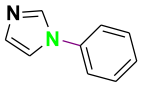	5	88

[a] Reaction conditions: aryl amine (1 mmol), aryl boronic acid (1 mmol), K_2CO_3 (1 eq.), Ni@Fe_3O_4–NDCs (0.1 g) in H_2O (5 mL) at 100 °C.
[b] Column chromatography yield.

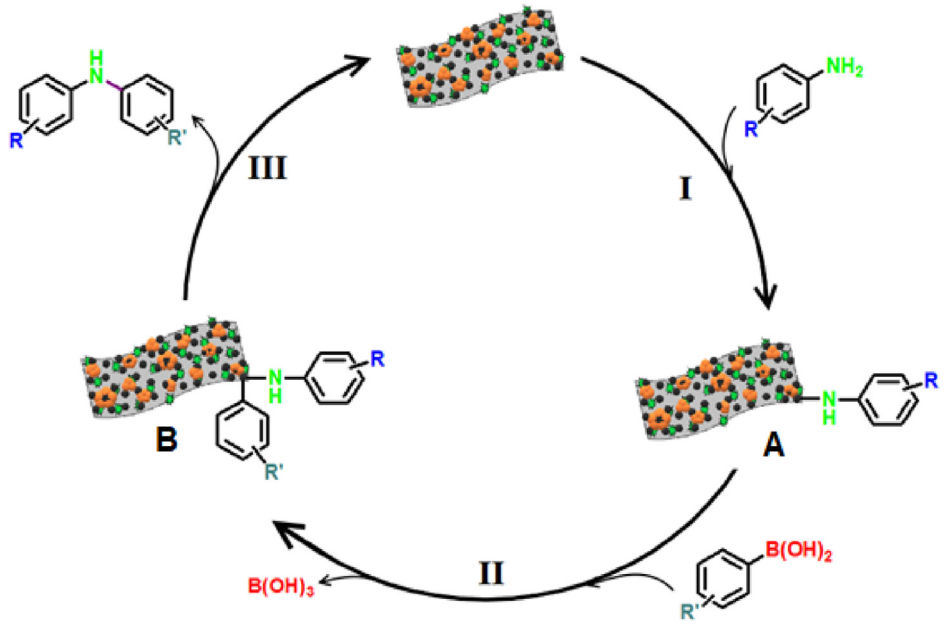

Fig. 10. Plausible mechanism for Ni catalyzed C–N bond formation.

methodology to synthesize various substituted diarylamines by the coupling of different aryl amines, alkyl amines and imidazole (heterocyclic amine) with aryl boronic acids as depicted in Table 3. It was found that all the para-substituted arylamines including both electron-deficient as well as electron-donating groups underwent clean conversion to give the desired products in good yields, whereas meta-substituted arylamines require long reaction time for the completion of the reaction (Table 3, entry 3, 14). It is remarkable to state that steric hindrance in the vicinity of the amino functionality had a significant influence on the C–N coupling reaction (Table 3, entry 4). Thus, ortho-substituted anilines were observed to be less acceptable substrates. Interestingly, all the examined boronic acids underwent clean conversion to give the desired coupling products (Table 3, entries 7–17) in good yields. The electronic nature or the substitution pattern did not have much effect on the cross-coupling reaction as both types of groups have lesser reactivity as compared to their unsubstituted counterpart. Additionally, to sightsee the scope of this method, the C–N cross-coupling reaction of other amines (alkylamines and imidazole) with phenylboronic acid was investigated (Table 3, entries 18–20) and we obtained the desired product in good yield in case of imidazole, whereas poor results were obtained in case of alkylamines. All the products were fully characterized by ^1H and ^{13}C NMR spectral data.

3.3. Proposed mechanism

Since, the monometallic nickel catalyst has shown enhanced catalytic activity and the corresponding XPS spectrum indicates the presence of pure Ni(II) species. This clearly signifies that Ni(II) is the active species in Chan-Lam cross-coupling. Further, HRTEM and XRD confirmed that Ni(II) is present in the form of nickel ferrites which resulted in improved morphology and enlarged surface area as authenticated by SEM and BET. These features have made the mono-metallic nickel catalyst more efficient than the bi-metallic catalyst due to the exposure of more surface-active sites. Based on this analysis, a proposed mechanism for the C–N cross-coupling reaction between phenyl boronic acid and aromatic amines is presented in Fig. 10. The reaction was proposed to proceed through a catalytic cycle involving coordination between Ni(II) and an amine (**I**) to give **A**. The second step could be transmetallation (**II**) of **A**

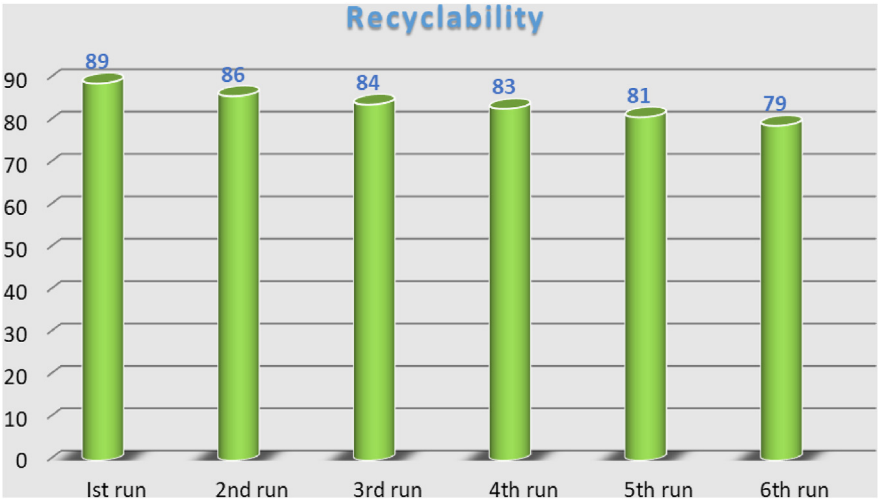

Fig. 11. Recyclability of Ni@Fe_3O_4–NDCs in C–N cross-coupling reaction.

Table 4
Comparison of earlier reported methods of Chan-Lam coupling with the present method.

S.No.	Catalyst used	Conditions	Time	Remarks	Ref
1	$NiCl_2{\cdot}6H_2O$, 2,2′-bipyridine	DBU, CH_3CN, RT	20–28 h	Homogeneous catalyst, use of ligand, longer reaction time	[26]
2	Ni(II) bis-(2-acetylthiophene) oxaloyldihydrazone	DBU, CH_3CN, 40 °C	15 h	Expensive, tedious synthesis, longer reaction time	[44]
3	$[Ni(COD)_2]$, IPr·HCl	NaO(*t*-Bu), toluene, 100 °C	20 h	Homogeneous catalyst, use of ligand, longer reaction time	[73]
4	$Ni(OAc)_2.4H_2O$, *N*-(pyridin-2-yl)benzamide	TMG, toluene, 60 °C	24–30 h	Homogeneous catalyst, use of ligand, longer reaction time	[46]
5	(BINAP)Ni-$[P(OPh)_3]_2$	NaO(*t*-Bu), toluene, 80 °C	18 h	Homogeneous catalyst, longer reaction time	[74]
6	$[Ni(IPr)]_2$ $(\mu\text{-}Cl)_2$, PPh_3/pyridine	NaO(*t*-Bu), THF, 40 °C	24 h	Homogeneous catalyst, use of ligand, longer reaction time	[75]
7	(PAd-DalPhos) Ni(*o*-tolyl)Cl	NaO(*t*-Bu), toluene, 25–140 °C	16 h	Homogeneous catalyst, use of ligand, longer reaction time	[27]
8	[SiCCSi]$NiBr_2$, $AgBPh_4$	KO(*t*-Bu), dioxane, 100 °C	25 h	Homogeneous catalyst, need of promoter, longer reaction time	[76]
9	$[Ni(COD)_2]$, 1,2-bis(dicyclohexyl-phosphino) benzene	NaO(*t*-Bu), toluene, 120 °C	20 h	Homogeneous catalyst, use of ligand, longer reaction time	[77]
10	(NHP-DalPhos)NiCl(*o*-tolyl)	NaO(*t*-Bu), toluene, 25–80 °C	16 h	Homogeneous catalyst, use of ligand, longer reaction time	[78]
11	Fe_3O_4@SiO_2/APTES/IMMPh@Ni^{2+}	Na_3PO_4, water, 80 °C	3–5 h	Heterogeneous catalyst, use of 3 eq. of amine	[47]
12	Ni@Fe_3O_4-NDCs	K_2CO_3, water, 100 °C	3–6 h	Inexpensive magnetically recoverable catalyst, use of mild conditions	Present work

with the arylboronic acid to form **B**. While the subsequent reductive elimination step (**III**) offered the corresponding *N*-arylated product.

3.4. Recyclability

Recyclability of Ni@Fe_3O_4–NDCs was examined for the C–N cross-coupling reaction using 4–methoxyaniline and phenyl boronic acid (Table 3, entry 2). After the end of the reaction, the catalyst was recovered using a magnet followed by washing with deionized water (3 × 10 mL), ethyl acetate (3 × 10 mL) and dried under a vacuum. Then a fresh reaction was carried out with the recovered catalyst and we didn't find any notable change in the catalytic activity up to six consecutive runs (Fig. 11) and therefore, the catalyst could be utilized at least six times without any substantial loss in activity. Further, to prove heterogeneity of synthesized catalyst and to eliminate any chance of leaching of the active metal species from the catalyst surface, a reaction (Table 3, entry 2) was accomplished until the conversion was up to 55% (1.5 h) and thereupon, the catalyst was removed via an external magnet and the liquid phase was again allowed to react under similar reaction conditions. We found no further increase in the conversion of the reactants in the resultant supernatant, thus omitting the chance of leaching of Ni nanoparticles which strongly advocates the catalysts heterogeneity. Besides, the XPS analysis of the reused Ni@Fe_3O_4–NDCs after 6^{th} run was also carried out to analyze the surface metal nanoparticles (Fig. 7). It was found that the oxidation state, as well as metal nanoparticle concentration, was almost the same even after the 6^{th} catalytic run, thus indicating the stability and heterogeneity of the catalyst.

3.5. Comparison of Ni@Fe_3O_4-NDCs with other reported catalytic systems

To show the supremacy of our present catalytic system as compared to the reported methodologies, the efficiency of the present method is compared with the earlier approaches for Chan-Lam coupling using nickel based catalysts (Table 4). From Table 4, it can be concluded that in the present protocol we have synthesized the substituted biaryl amines by using inexpensive, air stable, magnetically retrievable and recyclable catalyst under greener and mild reaction conditions and also, we get the products in good yield in lesser time. The present protocol involves the

use of mild base and equivalent amount of amine in green solvent (water) as compared to the reported methods. All these points together prove the higher efficiency of our catalytic system than the previously reported ones.

4. Conclusions

In summary, we have established an efficient strategy for the immobilization of metal nanoparticles on binder-free magnetic and nitrogen functionalities rich carbon support material. Eco-friendly, economical and magnetically recoverable nickel and/or iron supported five different catalysts were synthesized and their catalytic activity was tested for Chan-Lam cross-coupling using green and environmentally sustainable methodology. Satisfactory results were obtained with two catalysts-Ni@Fe–Fe_3O_4–NDCs and Ni@Fe_3O_4-NDCs, with the monometallic counterpart possessing unexpected enhanced catalytic activity. The better catalytic performance of monometallic catalyst is explained by means of various characterization techniques. Better morphology, high surface area and greater number of surface-active sites are the features possessed by the monometallic Ni-catalyst over the bimetallic one, which makes the former catalyst more active for Chan-Lam cross coupling. Despite following the same procedure for both the catalysts, the difference in surface properties is attributed to the difference in interactions between the Ni NPs and supported Fe_3O_4 material. In the monometallic catalyst, there exist strong interaction between Ni NPs and supported Fe_3O_4 material which leads to the formation of $NiFe_2O_4$, as evident by HRTEM, XPS and XRD, with improved surface properties. However, bimetallic catalyst does not form Ni ferrites which might be accredited to the interference of metallic Fe. Thus, in this report, the effect of interaction of Ni NPs with supported Fe_3O_4 material, with and without metallic iron, is systematically explored, which is found to be directly related to the morphology, surface area, surface active sites and finally the catalytic activity of the resultant catalyst. Furthermore, green and ligand-free reaction conditions, good catalytic activity, reusability, ease of recovery and the use of inexpensive metals make the reported procedure worthful from an environmental and industrial perspective. Such work could serve as a good step in designing efficient Ni catalysts with better morphology and enhanced catalytic activity.

CRediT authorship contribution statement

Chandan Sharma: Conceptualization, Data curation, Formal analysis, Funding acquisition, Investigation, Methodology, Software. **Nitika Sharma:** Data curation, Formal analysis, Investigation, Software. **Shally Sharma:** Formal analysis, Investigation, Software. **Surbhi Sharma:** Formal analysis, Investigation. **Satya Paul:** Conceptualization, Data curation, Formal analysis, Investigation, Methodology, Project administration, Software, Supervision, Validation, Visualization.

Declaration of competing interest

The authors declare that they have no known competing financial interests or personal relationships that could have appeared to influence the work reported in this paper.

Acknowledgements

We thank the Head, SAIF, IIT Bombay for HR–TEM, SEM, ICP–AES and EDX studies; Head, SAIF, Chandigarh for XRD; Head, ACMS, IIT Kanpur for XPS study and Head, CIF, Guwahati for VSM analysis. Financial support from DST (PURSE), RUSA (MHRD) and to authors, CS (SRF, UGC, New Delhi) and NS and SS (RUSA 2.0) is gratefully acknowledged.

Appendix B. Supplementary data

Supplementary data to this article can be found online at https://doi.org/10.1016/j.crgsc.2021.100133.

Appendix A. Supplementary data

The data that supports the findings of this study are available in the supporting information of this article.

References

[1] M. Ashraf, I. Khan, M. Usman, A. Khan, S.S. Shah, A.Z. Khan, K. Saeed, M. Yaseen, M.F. Ehsan, M.N. Tahir, N. Ullah, Hematite and magnetite nanostructures for green and sustainable energy harnessing and environmental pollution control: a review, Chem. Res. Toxicol. 33 (2020) 1292–1311.
[2] R.B.N. Baig, R.S. Varma, Magnetically retrievable catalysts for organic synthesis, Chem. Commun. 49 (2013) 752–770.
[3] M.B. Gawande, P.S. Branco, R.S. Varma, Nano-magnetite (Fe_3O_4) as a support for recyclable catalysts in the development of sustainable methodologies, Chem. Soc. Rev. 42 (2013) 3371–3393.
[4] N.A. Frey, S. Peng, K. Cheng, S. Sun, Magnetic nanoparticles: synthesis, functionalization, and applications in bioimaging and magnetic energy storage, Chem. Soc. Rev. 38 (2009) 2532–2542.
[5] W. Zhang, K. Banerjee-Ghosh, F. Tassinari, R. Naaman, Enhanced electrochemical water splitting with chiral molecule-coated Fe_3O_4 nanoparticles, ACS Energy Lett 3 (2018) 2308–2313.
[6] S.A. Adams, J.L. Hauser, A.C. Allen, K.P. Lindquist, A.P. Ramirez, S. Oliver, J.Z. Zhang, Fe_3O_4@SiO_2 nanoparticles functionalized with gold and poly(vinylpyrrolidone) for bio-separation and sensing applications, ACS Appl. Nano Mater. 1 (2018) 1406–1412.
[7] H. Hou, X. Huang, G. Wei, F. Xu, Y. Wang, S. Zhou, Fenton reaction-assisted photodynamic therapy for cancer with multifunctional magnetic nanoparticles, ACS Appl. Mater. Interfaces 11 (2019) 29579–29592.
[8] R.K. Sharma, S. Dutta, S. Sharma, R. Zboril, R.S. Varma, M.B. Gawande, Fe_3O_4 (iron oxide)-supported nanocatalysts: synthesis, characterization and applications in coupling reactions, Green Chem. 18 (2016) 3184–3209.
[9] H.M.A. Sharif, A. Mahmood, H.Y. Cheng, R. Djellabi, J. Ali, W.L. Jiang, S.S. Wang, M.R. Haider, N. Mahmood, A.J. Wang, Fe_3O_4 nanoparticles coated with EDTA and Ag nanoparticles for the catalytic reduction of organic dyes from wastewater, ACS Appl. Nano Mater. 2 (2019) 5310–5319.
[10] J. He, Y. Zhang, Q. Yuan, H. Liang, Catalytic activity and application of immobilized chloroperoxidase by biometric magnetic nanoparticles, Ind. Eng. Chem. Res. 58 (2019) 3555–3560.
[11] L. Huang, Q. Shuai, Facile approach to prepare sulfur-functionalized magnetic amide-linked organic polymers for enhanced Hg (II) removal from water, ACS Sustain. Chem. Eng. 7 (2019) 9957–9965.
[12] H. Wang, H. Tang, C. Yang, Y. Li, Selective single molecule nanopore sensing of microRNA using PNA functionalized magnetic core–shell Fe_3O_4–Au nanoparticles, Anal. Chem. 91 (2019) 7965–7970.
[13] A. Kong, P. Wang, H. Zhang, F. Yang, S. Huang, Y. Shan, One-pot fabrication of magnetically recoverable acid nanocatalyst, heteropolyacids/chitosan/Fe_3O_4, and its catalytic performance, Appl. Catal. Gen. 418 (2012) 183–189.
[14] M. Masteri-Farahani, N. Tayyebi, A new magnetically recoverable nanocatalyst for epoxidation of olefins, J. Mol. Catal. Chem. 348 (2011) 83–87.
[15] X. Cui, Y. Zheng, M. Tian, Z. Dong, Palladium nanoparticles supported on SiO_2@Fe_3O_4@m-MnO_2 mesoporous microspheres as a highly efficient and recyclable catalyst for hydrodechlorination of 2,4-dichlorophenol and reduction of nitroaromatic compounds and organic dyes, Mol. Catal. 433 (2017) 202–211.
[16] Y. Zhang, M. Zhang, J. Yang, L. Ding, J. Zheng, J. Xu, S. Xiong, Formation of Fe_3O_4@SiO_2@C/Ni hybrids with enhanced catalytic activity and histidine-rich protein separation, Nanoscale 8 (2016) 15978–15988.
[17] M. Kaur, C. Sharma, N. Sharma, B. Jamwal, S. Paul, Pd nanoparticles decorated on ZnO/Fe_3O_4 cores and doped with Mn^{2+} and Mn^{3+} for catalytic C–C coupling, nitroaromatics reduction, and the oxidation of alcohols and hydrocarbons, ACS Appl. Nano Mater. 3 (2020) 10310–10325.
[18] Y. Li, Z. Zhang, J. Shen, M. Ye, Hierarchical nanospheres based on Pd nanoparticles dispersed on carbon coated magnetite cores with a mesoporous ceria shell: a highly integrated multifunctional catalyst, Dalton Trans. 44 (2015) 16592–16601.
[19] X. Cui, W. Zuo, M. Tian, Z. Dong, J. Ma, Highly efficient and recyclable Ni MOF-derived N-doped magnetic mesoporous carbon-supported palladium catalysts for the hydrodechlorination of chlorophenols, J. Mol. Catal. Chem. 423 (2016) 386–392.
[20] Z. Wu, C. Sun, Y. Chai, M. Zhang, Fe_3O_4@SiO_2@Pd-Au: a highly efficient and magnetically separable catalyst for liquid-phase hydrodechlorination of 4-chlorophenol, RSC Adv. 1 (2011) 1179–1182.
[21] J. Bariwal, E.V. Eycken, C–N bond forming cross-coupling reactions: an overview, Chem. Soc. Rev. 42 (2013) 9283–9303.
[22] Y. Hirai, Y. Uozumi, Clean synthesis of triarylamines: Buchwald–Hartwig reaction in water with amphiphilic resin-supported palladium complexes, Chem. Commun. 46 (2010) 1103–1105.

[23] S. Sa, M.B. Gawande, A. Velhinho, J.P. Veiga, N. Bundaleski, J. Trigueiro, A. Tolstogouzov, O.M.N.D. Teodoro, R. Zboril, R.S. Verma, P.S. Branco, Magnetically recyclable magnetite–palladium (Nanocat-Fe–Pd) nanocatalyst for the Buchwald–Hartwig reaction, Green Chem. 16 (2014) 3494–3500.

[24] K. Kubota, T. Seo, K. Koide, Y. Hasegawa, H. Ito, Olefin-accelerated solid-state C–N cross-coupling reactions using mechanochemistry, Nat. Commun. 10 (2019) 111.

[25] P. Ruiz-Castillo, S.L. Buchwald, Applications of palladium-catalyzed C–N cross-coupling reactions, Chem. Rev. 11 (2016) 12564–12649.

[26] D.S. Raghuvanshi, A.K. Gupta, K.N. Singh, Nickel-mediated N-arylation with arylboronic acids: an avenue to Chan–Lam coupling, Org. Lett. 14 (2012) 4326–4329.

[27] C.M. Lavoie, M. Stradiotto, Bisphosphines: a prominent ancillary ligand class for application in nickel-catalyzed C–N cross-coupling, ACS Catal. 8 (2018) 7228–7250.

[28] J. Serra, T. Parella, X. Ribas, Au(III)-aryl intermediates in oxidant-free C–N and C–O cross-coupling catalysis, Chem. Sci. 8 (2017) 946–952.

[29] M.O. Akram, A. Das, I. Chakrabarty, N.T. Patil, Ligand-enabled gold-catalyzed C(sp^2)–N cross-coupling reactions of aryl iodides with amines, Org. Lett. 21 (2019) 8101–8105.

[30] S.Y. Moon, J. Nam, K. Rathwell, W.S. Kim, Copper-catalyzed Chan–Lam coupling between sulfonyl azides and boronic acids at room temperature, Org. Lett. 16 (2014) 338–341.

[31] M.A. Nasseri, Z. Rezazadeh, M. Kazemnejadi, A. Allahresani, A Co–Cu bimetallic magnetic nanocatalyst with synergistic and bifunctional performance for the base-free Suzuki, Sonogashira, and C–N cross-coupling reactions in water, Dalton Trans. 49 (2020) 10645–10660.

[32] F. Ullmann, J. Bielecki, Ueber synthesen in der biphenylreihe, Chem. Ber. 34 (1901) 2174–2185.

[33] F. Ullmann, Ueber eine neue Bildungsweise von Diphenylamin derivaten, Chem. Ber. 36 (1903) 2382–2384.

[34] F. Ullmann, P. Sponagel, Ueber die phenylirung von phenolen, Chem. Ber. 38 (1905) 2211–2212.

[35] I. Goldberg, Ueber phenylirungen bei gegenwart von kupfer als katalysator, Chem. Ber. 39 (1906) 1691–1692.

[36] J. Louie, J.F. Hartwig, Palladium-catalyzed synthesis of arylamines from aryl halides. Mechanistic studies lead to coupling in the absence of tin reagents, Tetrahedron Lett. 36 (1995) 3609–3612.

[37] A.S. Guram, R.A. Rennels, S.L. Buchwald, A simple catalytic method for the conversion of aryl bromides to arylamines, Angew. Chem., Int. Ed. Engl. 34 (1995) 1348–1350.

[38] D.S. Surry, S.L. Buchwald, Biaryl phosphane ligands in palladium-catalyzed amination, Angew. Chem. Int. Ed. 47 (2008) 6338–6361.

[39] A. Correa, C. Bolm, Iron-catalyzed N-arylation of nitrogen nucleophiles, Angew. Chem. Int. Ed. 46 (2007) 8862–8865.

[40] O. Bistri, A. Correa, C. Bolm, Iron-catalyzed C-O cross-couplings of phenols with aryl iodides, Angew. Chem. Int. Ed. 47 (2008) 586–588.

[41] G. Toma, R. Yamaguchi, Cobalt-catalyzed C–N bond-forming reaction between chloronitrobenzenes and secondary amines, Eur. J. Org Chem. (2010) 6404–6408.

[42] P. Saha, M.A. Ali, P. Ghosh, T. Punniyamurthy, Cobalt-catalyzed intramolecular C–N and C–O cross-coupling reactions: synthesis of benzimidazoles and benzoxazoles, Org. Biomol. Chem. 8 (2010) 5692–5699.

[43] B.Y.H. Tan, Y.C. Teo, Efficient cobalt-catalyzed C–N cross-coupling reaction between benzamide and aryl iodide in water, Org. Biomol. Chem. 12 (2014) 7478–7481.

[44] D.P. Singh, D.S. Raghuvanshi, K.N. Singh, V.P.J. Singh, Synthesis, characterization and catalytic application of some novel binuclear transition metal complexes of bis-(2-acetylthiophene) oxaloyldihydrazone for C–N bond formation, J. Mol. Catal. Chem. 379 (2013) 21–29.

[45] J. Shi, F.L. Li, H.X. Li, F. Wang, H. Yua, Z.G. Ren, W.H. Zhang, J.P. Lang, Nickel(II) thiolates derived from transmetallation reaction of $[Zn(Tab)_4](PF_6)_2$ with Ni(II) ions and their catalytic activity toward the C–N coupling reactions, Inorg. Chem. Commun. 46 (2014) 159–162.

[46] S. Keesara, N-(pyridin-2-yl) benzamide: efficient ligand for the nickel catalyzed Chan–Lam cross-coupling reaction, Tetrahedron Lett. 56 (2015) 6685–6688.

[47] M.S. Nejad, N. Seyedi, H. Sheibani, S. Behzadi, Synthesis and characterization of Ni(II) complex functionalized silica-based magnetic nanocatalyst and its application in C–N and C–C cross-coupling reactions, Mol. Divers. 23 (2019) 527–539.

[48] C. Sharma, M. Kaur, A. Choudhary, S. Sharma, S. Paul, Nitrogen doped carbon–silica based Cu(0) nanometal catalyst enriched with well-defined N-moieties: synthesis and application in one-pot synthesis of 1,4-disubstituted-1,2,3-triazoles, Catal. Lett. 150 (2019) 82–94.

[49] Z.P. Demko, K.B. Sharpless, Preparation of 5-substituted 1H-tetrazoles from nitriles in water, J. Org. Chem. 66 (2001) 7945–7950.

[50] H. Veisi, S. Sajjadifar, P.M. Biabri, S. Hemmati, Oxo-vanadium complex immobilized on chitosan coated-magnetic nanoparticles (Fe_3O_4): a heterogeneous and recyclable nanocatalyst for the chemoselective oxidation of sulfides to sulfoxides with H_2O_2, Polyhedron 153 (2018) 240–247.

[51] C. Li, Y. Wei, A. Liivat, Y. Zhu, J. Zhu, Microwave-solvothermal synthesis of Fe_3O_4 magnetic nanoparticles, Mater. Lett. 107 (2013) 23–26.

[52] H.Q. Alijani, S. Pourseyedi, M. Torkzadeh-Mahani, A. Seifalian, M. Khatami, Bimetallic nickel-ferrite nanorod particles: greener synthesis using rosemary and its biomedical efficiency, Artif. Cells Nanomed. Biotechnol. 48 (2020) 242–251.

[53] P. Moravec, J. Smolik, H. Keskinen, J.M. Makela, S. Bakardjieva, V.V. Levdansky, NiO_x nanoparticle synthesis by chemical vapor deposition from nickel acetylacetonate, Mater. Sci. Appl. 2 (2011) 258–264.

[54] Y. Du, H. Chen, R. Chen, N. Xu, Synthesis of p-aminophenol from p-nitrophenol over nano-sized nickel catalysts, Appl. Catal. Gen. 277 (2004) 259–264.

[55] Y. Li, Y. Hu, G. Huang, C. Li, Metallic iron nanoparticles: flame synthesis, characterization and magnetic properties, Particuology 11 (2013) 460–467.

[56] C. Liang, S. Huang, W. Zhao, W. Liu, J. Chen, H. Liu, Y. Tong, Polyhedral Fe_3O_4 nanoparticles for lithium ion storage, New J. Chem. 39 (2015) 2651–2656.

[57] J. Chen, Y. Liu, G. Zhu, A. Yuan, Ag@Fe_3O_4 nanowire: fabrication, characterization and peroxidise-like activity, Cryst. Res. Technol. 49 (2014) 309–314.

[58] Z. Hao, M. Fuji, J. Zhou, Diperovskite $(NH_4)_3FeF_6$/graphene nanocomposites for superior Na-ion storage, Sustain. Energy Fuels 3 (2019) 2828–2836.

[59] Q. Chen, R. Wang, F. Lu, X. Kuang, Y. Tong, X. Lu, Boosting the oxygen evolution reaction activity of $NiFe_2O_4$ nanosheets by phosphate ion functionalization, ACS Omega 4 (2019) 3493–3499.

[60] D. Kim, M. Jang, J. Seo, K.H. Nam, H. Han, S.B. Khan, UV-cured poly (urethane acrylate) composite films containing surface-modified tetrapod ZnO whiskers, Compos. Sci. Technol. 75 (2013) 84–92.

[61] S.B. Khan, K.A. Alamry, E.N. Bifari, A.M. Asiri, M. Yasir, L. Gzara, R.Z. Ahmad, Assessment of antibacterial cellulose nanocomposites for water permeability and salt rejection, J. Ind. Eng. Chem. 24 (2015) 266–275.

[62] Q. An, M. Yu, Y. Zhang, W. Ma, J. Guo C. Wang, Fe_3O_4@carbon microsphere supported Ag–Au bimetallic nanocrystals with the enhanced catalytic activity and selectivity for the reduction of nitroaromatic compounds, J. Phys. Chem. C 116 (2012) 22432–22440.

[63] H. Veisi, J. Gholami, H. Ueda, P. Mohammadi, M.J. Noroozi, Magnetically palladium catalyst stabilized by diaminoglyoxime-functionalized magnetic Fe_3O_4 nanoparticles as active and reusable catalyst for Suzuki coupling reactions, J. Mol. Catal. Chem. 396 (2015) 216–223.

[64] J. Ashok, S. Kawi, Nickel–iron alloy supported over iron–alumina catalysts for steam reforming of biomass tar model compound, ACS Catal. 4 (2014) 289–301.

[65] N. Dalai, B. Mohanty, A. Mitra, B. Jena, Highly active ternary nickel–iron oxide as bifunctional catalyst for electrochemical water splitting, Chemistry 4 (2019) 7791–7796.

[66] P. Cao, H.Y. Zhang, G. Yina, Y. Zhang, J. Zhao, Nitrogen doped carbon supported iron catalysts for highly selective production of 4,4′-diamino-2,2′-stilbenedisulfonic acid, Catal. Commun. 132 (2019) 105822.

[67] C. Marras, D. Loche, A. Corrias, Z. Konya, M.F. Casula, Bimetallic Fe/Mo–SiO_2 aerogel catalysts for catalytic carbon vapour deposition production of carbon nanotubes, J. Sol. Gel Sci. Technol. 73 (2015) 379–388.

[68] H. Veisi, A. Rashtiani, A. Rostami, M. Shirinbayan, S. Hemmati, Chemo-selective oxidation of sulfide to sulfoxides with H_2O_2 catalyzed by oxo-vanadium/Schiff-base complex immobilized on modified magnetic Fe_3O_4 nanoparticles as a heterogeneous and recyclable nanocatalyst, Polyhedron 157 (2019) 358–366.

[69] Q. Ding, H. Liu, L. Yang, J. Liu, Speedy and surfactant-free in situ synthesis of nickel/Ag nanocomposites for reproducible SERS substrates, J. Mater. Chem. 22 (2012) 19932–19939.

[70] R.K. Dhokale, H.M. Yadav, S.N. Achary, S.D. Delekar, Anatase supported nickel nanoparticles for catalytic hydrogenation of 4-nitrophenol, Appl. Surf. Sci. 303 (2014) 168–174.

[71] P. Mishra, A. Behera, D. Kandi, S. Ratha, K. Parida, Novel magnetic retrievable visible-light-driven ternary Fe_3O_4@$NiFe_2O_4$/Phosphorus-doped g-C_3N_4 nanocomposite photocatalyst with significantly enhanced activity through a double-Z-scheme system, Inorg. Chem. 59 (2020) 4255–4272.

[72] M. Islam, G. Ali, M.G. Jeong, W. Choi, K.Y. Chung, H.G. Jung, Study on the electrochemical reaction mechanism of $NiFe_2O_4$ as a high-performance anode for Li-ion batteries, ACS Appl. Mater. Interfaces 9 (2017) 14833–14843.

[73] F. Zhu, Z.X. Wang, Nickel-catalyzed coupling of fluoroarenes and amines, Adv. Synth. Catal. 355 (2013) 3694–3702.

[74] S.S. Kampmann, B.W. Skelton, D.A. Wild, G.A. Koutsantonis, S.G. Stewart, An air-stable nickel(0) phosphite precatalyst for primary alkylamine C–N cross-coupling reactions, Eur. J. Org Chem. (2015) 5995–6004.

[75] K. Matsubara, Y. Fukahori, T. Inatomi, S. Tazaki, Y. Yamada, Y. Koga, S. Kanegawa, T. Nakamura, Monomeric three-coordinate N-heterocyclic carbene nickel(I) complexes: synthesis, structures, and catalytic applications in cross-coupling reactions, Organometallics 35 (2016) 3281–3287.

[76] Y.P. Zhou, S. Raoufmoghaddam, T. Szilvasi, M. Driess, A bis(silylene)-substituted ortho-carborane as a superior ligand in the nickel-catalyzed amination of arenes, Angew. Chem. 128 (2016) 13060–13064.

[77] T. Harada, Y. Ueda, T. Iwai, M. Sawamura, Nickel-catalyzed amination of aryl fluorides with primary amines, Chem. Commun. 54 (2018) 1718–1721.

[78] A.V. Gatien, C.M. Lavoie, R.N. Bennett, M.J. Ferguson, R. McDonald, E.R. Johnson, A.W. Speed, M. Stradiotto, Application of diazaphospholidine/diazaphospholene-based bisphosphines in room-temperature nickel-catalyzed C(sp^2)–N cross-couplings of primary alkylamines with (hetero) aryl chlorides and bromides, ACS Catal. 8 (2018) 5328–5339.